Article

Modeling [Fe–Fe] Hydrogenase: Evidence for Bridging Carbonyl and Distal Iron Coordination Vacancy in an Electrocatalytically Competent Proton Reduction by an Iron Thiolate Assembly That Operates through Fe(0)–Fe(II) Levels

Mun Hon Cheah, Cdric Tard, Stacey J. Borg, Xiaoming Liu, Saad K. Ibrahim, Christopher J. Pickett, and Stephen P. Best

J. Am. Chem. Soc., **2007**, 129 (36), 11085-11092• DOI: 10.1021/ja071331f • Publication Date (Web): 18 August 2007

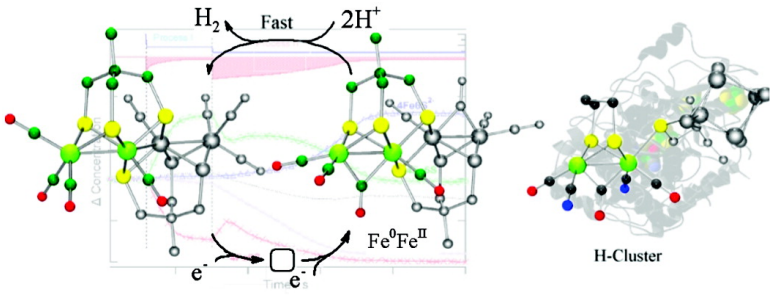

More About This Article

Additional resources and features associated with this article are available within the HTML version:

- Supporting Information
- Links to the 15 articles that cite this article, as of the time of this article download
- Access to high resolution figures
- Links to articles and content related to this article
- Copyright permission to reproduce figures and/or text from this article

View the Full Text HTML

J|A|C|S
ARTICLES
Published on Web 08/18/2007

Modeling [Fe−Fe] Hydrogenase: Evidence for Bridging Carbonyl and Distal Iron Coordination Vacancy in an Electrocatalytically Competent Proton Reduction by an Iron Thiolate Assembly That Operates through Fe(0)−Fe(II) Levels

Mun Hon Cheah,[†] Cédric Tard,[‡] Stacey J. Borg,[†] Xiaoming Liu,[‡] Saad K. Ibrahim,[‡] Christopher J. Pickett,*[,‡] and Stephen P. Best*[,†]

Contribution from the School of Chemistry, University of Melbourne, Victoria, Australia, 3010, and School of Chemical Sciences & Pharmacy, University of East Anglia, Norwich, NR4 7TJ

Received February 25, 2007; E-mail: spbest@unimelb.edu.au; c.pickett@uea.ac.uk

Abstract: IR spectroelectrochemistry of $Fe_4\{Me(CH_2S)_3\}_2(CO)_8$ (**4Fe6S**) in the ν(CO) region shows that the neutral and anion forms have all their CO groups terminally bound to the Fe atoms; however, for the dianion there is a switch of the coordination mode of at least one of the CO groups. The available structural and ν(CO) spectra are closely reproduced by density-functional theory calculations. The calculated structure of **4Fe6S**$^{2-}$ closely mirrors that of the diiron subsite of the [Fe−Fe] hydrogenase H cluster with a bridging CO group and an open coordination site on the outer Fe atom of pairs of dithiolate-bridged Fe^0Fe^{II} subunits connected by two bridging thiolates. Geometry optimization based on the all-terminal CO isomer of **4Fe6S**$^{2-}$ does not give a stable structure but reveals a second-order saddle point ca. 11.53 kcal mol^{-1} higher in energy than the CO-bridged form. Spectroelectrochemical studies of electrocatalytic proton reduction by **4Fe6S** show that slow turnover from the primary reduction process ($E_{1/2}' = -0.71$ V vs Ag/AgCl) involves rate-limiting protonation of **4Fe6S**$^{-}$ followed by reduction to H:**4Fe6S**$^{-}$. Rapid electrocatalytic proton reduction is obtained at potentials sufficient to access **4Fe6S**$^{2-}$, where the rate of dihydrogen elimination from the $Fe^{II}Fe^{II}$ core of **4Fe6S** is ca. 500 times faster than that from the $Fe^{I}Fe^{I}$ core of $Fe_2(\mu\text{-}S(CH_2)_3S)(CO)_6$. The dramatically increased rate of electrocatalysis obtained from **4Fe6S** over all previously identified model compounds appears to be related to the features uniquely common between it and the H-cluster, namely, that turnover involves the same formal redox states of the diiron unit ($Fe^{I}Fe^{II}$ and Fe^0Fe^{II}), the presence of an open site on the outer Fe atom of the Fe^0Fe^{II} unit, and the thiolate-bridge to a second one-electron redox unit.

Introduction

Notwithstanding the uncertainty remaining over the exact identity of the central light atom of the dithiolate bridge and the CO/CN arrangement, the structure of the catalytic center of the [Fe−Fe] hydrogenase enzyme is well-established by X-ray crystallographic[1−3] and spectroscopic[3−5] investigations. These results provide a framework for the development and evaluation of computational methods for describing the system. In this regard, density functional theory (DFT) has been shown to be extremely effective in terms of reproducing both the structure and spectroscopic details of closely related diiron compounds.[6−9] Importantly, these approaches offer the possibility of charting the reaction path or, more properly, providing a quantitative basis for excluding alternative reaction schemes.

Deliberation on the reaction path for dihydrogen oxidation has focused on the open coordination site of Fe_d (Scheme 1), the site of CO binding in the CO inhibited form of the enzyme.[12] Both $[2Fe]_{H_{ox}}$ and its one-electron-reduced analogue, $[2Fe]_{H_{red}}$, have similar structures, although in the latter case there is a weak interaction between Fe_p and the bridging CO group to give an up:down edge-shared bi-square pyramidal geometry.[1,3,13] Activation of dihydrogen may proceed by dihydrogen binding

[†] University of Melbourne.
[‡] University of East Anglia.

(1) Nicolet, Y.; Piras, C.; Legrand, P.; Hatchikian, C. E.; Fontecilla-Camps, J. C. *Structure* **1999**, *7*, 13−23.
(2) Peters, J. W.; Lanzilotta, W. N.; Lemon, B. J.; Seefeldt, L. C. *Science* **1998**, *282*, 1853−8.
(3) Nicolet, Y.; de Lacey, A. L.; Vernede, X.; Fernandez, V. M.; Hatchikian, E. C.; Fontecilla-Camps, J. C. *J. Am. Chem. Soc.* **2001**, *123*, 1596−601.
(4) Pierik, A. J.; Hulstein, M.; Hagen, W. R.; Albracht, S. P. J. *Eur. J. Biochem.* **1998**, *258*, 572−8. Chen, Z.; Lemon, B. J.; Huang, S.; Swartz, D. J.; Peters, J. W.; Bagley, K. A. *Biochemistry* **2002**, *41*, 2036−43.
(5) de Lacey, A. L.; Stadler, C.; Cavazza, C.; Hatchikian, E. C.; Fernandez, V. M. *J. Am. Chem. Soc.* **2000**, *122*, 11232−3.
(6) Fiedler, A. T.; Brunold, T. C. *Inorg. Chem.* **2005**, *44*, 9322−34. Zilberman, S.; Stiefel, E. I.; Cohen, M. H.; Car, R. *J. Phys. Chem. B* **2006**, *110*, 7049−57. Tye, J. W.; Darensbourg, M. Y.; Hall, M. B. *J. Comput. Chem.* **2006**, *27*, 1454−62. Bruschi, M.; Zampella, G.; Fantucci, P.; De Gioia, L. *Coord. Chem. Rev.* **2005**, *249*, 1620−40. Zilberman, S.; Stiefel, E. I.; Cohen, M. H.; Car, R. *Inorg. Chem.* **2006**, *45*, 5715−7.
(7) Fiedler, A. T.; Brunold, T. C. *Inorg. Chem.* **2005**, *44*, 1794−809.
(8) Bruschi, M.; Fantucci, P.; De Gioia, L. *Inorg. Chem.* **2002**, *41*, 1421−9.
(9) Borg, S. J.; Tye, J. W.; Hall, M. B.; Best, S. P. *Inorg. Chem.* **2007**, *46*, 384−94.
(10) Cao, Z.; Hall, M. B. *J. Am. Chem. Soc.* **2001**, *123*, 3734−42. Fan, H.-J.; Hall, M. B. *J. Am. Chem. Soc.* **2001**, *123*, 3828−9. Liu, Z.-P.; Hu, P. *J. Chem. Phys.* **2002**, *117*, 8177−80. Liu, Z.-P.; Hu, P. *J. Am. Chem. Soc.* **2002**, *124*, 5175−82.
(11) Zhou, T.; Mo, Y.; Liu, A.; Zhou, Z.; Tsai, K. R. *Inorg. Chem.* **2004**, *43*, 923−30.
(12) Lemon, B. J.; Peters, J. W. *Biochemistry* **1999**, *38*, 12969−73.

Scheme 1. Schematic Representation of $\mathbf{H_{ox}}$, the Catalytic Center of the Oxidized Form of [Fe−Fe] Hydrogenase, the Diiron Subsite, $[2Fe]_{H_{ox}}$, and Structures of Intermediates Associated with the Pathways for Dihydrogen Activation That Involve Dihydrogen Binding to (a) Fe_d[10] or (b) to Both Metal Atoms of the Diiron Subsite[8,11]

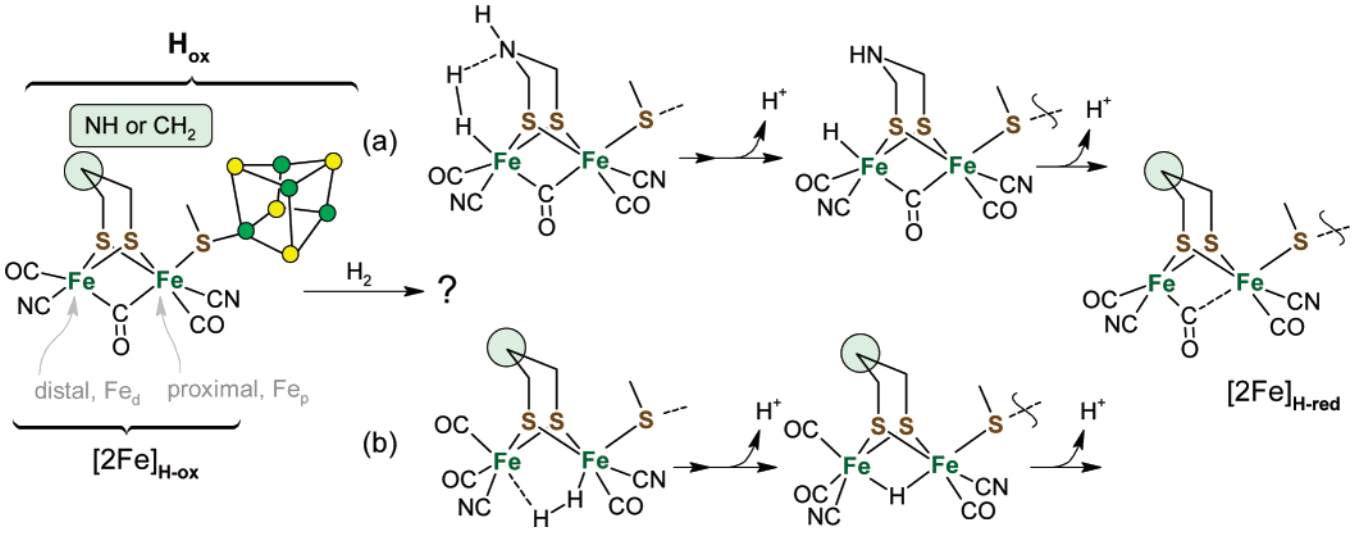

to this site (Scheme 1a). Heterolytic cleavage of bound dihydrogen would be assisted by interaction with the lone pair of the nitrogen atom of a di(thiomethyl)amine (dta) bridging ligand. DFT calculations suggest that such a path is energetically feasible,[10] and there is independent support for the assignment of the dta bridge based on analysis of the hydrogen-bonding interactions in the crystal.[5] An alternate reaction path may be proposed that involves dihydrogen binding to Fe_p where Fe_d interacts with the nonbonded hydrogen atom. In this case, dihydrogen binding is coupled with the bridging CO group adopting a terminal mode of coordination to Fe_d (Scheme 1b). DFT calculations suggest that this reaction path is also energetically feasible,[8,11] and a recent comparative study of the alternative proposals suggests that the energy differences are not sufficiently large for the DFT methods to allow exclusion of either alternative.[14]

There are excellent structural and functional models of the H-cluster, and progress in these areas has recently been reviewed.[15] For the most part, the focus has concentrated on $[2Fe]_{\mathbf{H}}$, where the most simple example, $Fe_2(\mu\text{-}S(CH_2)_3S)(CO)_6$ (**3S**), has been shown also to exhibit hydrogenase activity—at least in terms of electrocatalytic proton reduction.[16,17] Further elaboration by incorporation of a dta bridge,[18,19] regiospecific cyanation,[20] and site differentiation by incorporation of a pendant thioether or thiolate to the bridging ligand[19,21] yields close compositional analogues of the CO inhibited form of $[2Fe]_{\mathbf{H}}$ and an all-CO analog that incorporates both the **2Fe3S** and **4Fe4S** domains of $\mathbf{H_{ox}}$.[22] Spectroscopic and computational studies of ligand substitution reactions of diiron compounds related to $[2Fe]_{\mathbf{H}}$ suggest that a change in the mode of CO coordination facilitates ligand association/dissociation.[23,24] Simply, this allows the higher coordination intermediate to be accommodated by homolytic cleavage of the Fe−Fe bond while an 18-electron count is retained at both metal centers. However, these considerations do not provide a basis for distinction between the alternate pathways shown in Scheme 1. While a higher reactivity for terminally bound over bridging hydrides is suggested by studies of the isomers of $[HFe_2(\mu\text{-}S(CH_2)_2S)(CO)_2(PMe_3)_4]^+$ recently reported by Rauchfuss and co-workers,[25] the protonated forms of $[H_nFe_2(\mu\text{-}PPh_2)_2(CO)_6]^{n-2}$, n = 1 or 2, have terminally bound hydrides, and these are unreactive with protons.[26,27] Moreover, $Fe_2(\mu\text{-}PPh_2(CH_2)_3PPh_2)(CO)_6$ (**3P**) and **3S** undergo electrocatalytic proton reduction at similar rates, where the reaction path appears to involve a bridging hydride (i.e., the reverse of Scheme 1b).[28] This conclusion is supported by an independent DFT study of the reaction path for **3S**.[29] Central to the current investigation is the relative importance of bridging and terminally bound hydrides in the reaction path and, consequently, the role of the two iron atoms of $[2Fe]_{\mathbf{H}}$ in

(13) Nicolet, Y.; Lemon, B. J.; Fontecilla-Camps, J. C.; Peters, J. W. *Trends Biochem. Sci.* **2000**, *25*, 138−43.
(14) Zampella, G.; Greco, C.; Fantucci, P.; De Gioia, L. *Inorg. Chem.* **2006**, *45*, 4109−18.
(15) Liu, X.; Ibrahim, S. K.; Tard, C.; Pickett, C. J. *Coord. Chem. Rev.* **2005**, *249*, 1641−52. Capon, J.-F.; Gloaguen, F.; Schollhammer, P.; Talarmin, J. *Coord. Chem. Rev.* **2005**, *249*, 1664−76.
(16) Borg, S. J.; Behrsing, T.; Best, S. P.; Razavet, M.; Liu, X.; Pickett, C. J. *J. Am. Chem. Soc.* **2004**, *126*, 16988−99.
(17) Chong, D.; Georgakaki, I. P.; Mejia-Rodriguez, R.; Sanabria-Chinchilla, J.; Soriaga, M. P.; Darensbourg, M. Y. *Dalton Trans.* **2003**, 4158−63.
(18) Lawrence, J. D.; Li, H.; Rauchfuss, T. B.; Benard, M.; Rohmer, M.-M. *Angew. Chem., Int. Ed.* **2001**, *40*, 1768−71. Li, H.; Rauchfuss, T. B. *J. Am. Chem. Soc.* **2002**, *124*, 726−7.
(19) Lawrence, J. D.; Li, H.; Rauchfuss, T. B. *Chem. Commun.* **2001**, 1482−3.
(20) Lyon, E. J.; Georgakaki, I. P.; Reibenspies, J. H.; Darensbourg, M. Y. *Angew. Chem., Int. Ed.* **1999**, *38*, 3178−80. Cloirec, A. L.; Davies, S. C.; Evans, D. J.; Hughes, D. L.; Pickett, C. J.; Best, S. P.; Borg, S. *Chem. Commun.* **1999**, 2285−6. Schmidt, M.; Contakes, S. M.; Rauchfuss, T. B. *J. Am. Chem. Soc.* **1999**, *121*, 9736−7.
(21) Razavet, M.; Davies, S. C.; Hughes, D. L.; Pickett, C. J. *Chem. Commun.* **2001**, 847−8. Razavet, M.; Davies, S. C.; Hughes, D. L.; Barclay, J. E.; Evans, D. J.; Fairhurst, S. A.; Liu, X.; Pickett, C. J. *Dalton Trans.* **2003**, 586−95.
(22) Tard, C.; Liu, X.; Ibrahim Saad, K.; Bruschi, M.; De Gioia, L.; Davies, S. C.; Yang, X.; Wang, L.-S.; Sawers, G.; Pickett, C., J. *Nature* **2005**, *433*, 610−3.
(23) George, S. J.; Cui, Z.; Razavet, M.; Pickett, C. J. *Chem.—Eur. J.* **2002**, *8*, 4037−46.
(24) Boyke, C. A.; Rauchfuss, T. B.; Wilson, S. R.; Rohmer, M.-M.; Benard, M. *J. Am. Chem. Soc.* **2004**, *126*, 15151−60. Darensbourg, M. Y.; Lyon, E. J.; Zhao, X.; Georgakaki, I. P. *Proc. Natl. Acad. Sci. U.S.A.* **2003**, *100*, 3683−8. Zampella, G.; Bruschi, M.; Fantucci, P.; Razavet, M.; Pickett, C. J.; De Gioia, L. *Chem.—Eur. J.* **2005**, *11*, 509−20.
(25) van der Vlugt, J. I.; Rauchfuss, T. B.; Whaley, C. M.; Wilson, S. R. *J. Am. Chem. Soc.* **2005**, *127*, 16012−3.
(26) Cheah, M. H.; Borg, S. J.; Bondin, M. I.; Best, S. P. *Inorg. Chem.* **2004**, *43*, 5635−44.
(27) Dobbie, R. C.; Whittaker, D. *Chem. Commun.* **1970**, 796−7.
(28) Cheah, M. H.; Borg, S. J.; Best, S. P. *Inorg. Chem.* **2007**, *46*, 1741−50.
(29) Greco, C.; Zampella, G.; Bertini, L.; Bruschi, M.; Fantucci, P.; Gioia, L. D. *Inorg. Chem.* **2007**, *47*, 108−16.

dihydrogen activation (Scheme 1). Since the choreography of the reaction involves either CO or H bridging of the diiron centers, the reaction path may be considered from the perspective of either the H or CO groups.

The compound $Fe_4[MeC(SCH_2)_3]_2(CO)_8$ (**4Fe6S**), which is formed in the reaction of Bosnich's trithiol and $[Fe_3(CO)_{12}]$,[30] presents pairs of dithiolate-bridged diiron centers that feature markedly different coordination environments for the Fe atoms and promotes electrocatalytic proton reduction at relatively mild potentials and at a higher formal oxidation state for the Fe centers than for previously identified structural or functional models of $[2Fe]_{\mathbf{H}}$. The present investigation seeks to delineate the reduction chemistry of **4Fe6S** and to establish the relationships between this chemistry and that of $[2Fe]_{\mathbf{H}}$.

Experimental Section

Unless otherwise stated chemicals (Aldrich) and high-purity gases (BOC) were obtained from commercial sources and used without further purification. The ^{13}CO (99.2 atom %) was obtained from Trace Sciences International Corp., Ontario, Canada. Elemental analyses were performed by Medac Ltd, Egham, UK. Solvents were purified using standard procedures[31] and were distilled under a dinitrogen atmosphere immediately prior to use or transfer to a glove box (Vacuum Atmospheres). Tetra-n-butylammonium hexafluorophosphate (TBA-$[PF_6]$) was synthesized and purified using standard procedures[32] and lutidinium *p*-toluenesulfonate, LutH[OTs], was prepared by reaction of 2,6-dimethylpyridine (Lut) with the appropriate acid.

Synthesis of $Fe_4(CO)_8(CH_3C(CH_2S)_2)_2 \cdot {}^1/_2(CH_2Cl_2)$, 4Fe6S·$^1/_2(CH_2Cl_2)$. $Fe_3(CO)_{12}$ (3.0 g, 5.9 mmol) was dissolved in toluene (50 cm^3) and stirred. 1,1,1-Tris(mercaptomethyl)ethane (1.0 g, 5.9 mmol) was added and the solution was heated at 80 °C for 2 h. After solvent removal, the solid was purified by flash chromatography (diethyl ether and then dichloromethane) to give a dark brown solid (0.27 g, 0.3 mmol, 10%). This solid was recrystallized from dichloromethane to afford a shiny, microcrystalline brown-black material. ν_{max}/cm^{-1} (CO): 2046, 1988 and 1947 cm^{-1} (dichloromethane). NMR δ_H (400 MHz; solvent $CDCl_3$; standard $SiMe_4$): 0.94 (s, 6H, 2×CH_3), 1.16 (2H, d, *J* 14.2 Hz, 2×C*H*SFe), 1.59 (2H, d, *J* 14.2 Hz, 2×C*H*SFe), 1.97 (2H, d, *J* 13.9 Hz, 2×C*H*SFe), 2.13 (2H, d, *J* 13.2 Hz, 2×C*H*SFe), 2.77 (2H, d, *J* 13.7 Hz, 2×C*H*SFe), 3.54 (2H, d, *J* 13.7 Hz, 2×C*H*SFe), 5.32 (1H, 0.5 CH_2Cl_2). MS-FAB (NOBA matrix, *m*/*z*): M + H^+ 779. MS-ES+ (cone potential 50 V, solvent carrier $MeCN/CH_2Cl_2$ + ammonium acetate): M + H^+ 779, M + NH_4^+ 796. Anal. Calcd for $C_{18}H_{18}O_8S_6Fe_4 \cdot 1/2(CH_2Cl_2)$: C 27.08; H 2.33; S 23.4; Fe 27.2. Found: C 27.27; H 2.27; S 22.5; Fe 26.6.

Notes: The presence of 0.5 mol of dichloromethane per complex in the recrystallized material was confirmed by comparison of the integrated proton resonances for the complex with that for the solvate molecule in $CDCl_3$; experimental Fe and S analyses are somewhat low compared with theory, but this is not exceptional for this class of iron−sulfur compound,[33] where formation of metal sulfides can interfere in the analysis. Importantly, solution spectroscopic (FTIR, NMR) and electrochemical data reported above for the material used in this study is identical with that of structurally characterized **4Fe6S** prepared by the same method but isolated as homogeneous dark red needles from ethyl acetate/diethyl ether.[30]

Spectroelectrochemical (SEC) experiments were conducted using a purpose built cell previously described.[34] All experiments employed a 3 mm diameter vitreous carbon working electrode, silver pseudo-reference electrode, and platinum foil counter electrode. The potential of the reference electrode was estimated from the voltammetry of the solution under investigation and, by comparison with experiments conducted in the presence of ferrocene (Fc), all potentials are quoted relative to the Ag^+/AgCl reference electrode. Against this reference the Fc^+/Fc couple occurs at +0.51 V in CH_2Cl_2.[35] Solutions for SEC analysis were prepared under strictly anaerobic conditions either through the agency of a Vacuum Atmospheres glove box or using standard Schlenk techniques. The applied potential was controlled using a PAR model 362 potentiostat. A Powerlab 4/20 interface (ADInstruments) using EChem V1.5.2 or Chart V4.12 provided a means of setting the applied potential and monitoring the potential and current response during SEC experiments. IR spectra were obtained using a Bio-Rad FT175C FTIR equipped with a Ge/KBr beamsplitter and narrow band MCT detector. Spectral subtraction and curve fitting were performed using Grams/32 AI software (Galactic), and multicomponent analysis was conducted using routines available within Igor Pro (version 5.04B, Wavemetrics).

DFT calculations were carried out within the *Gaussion 03* (revision B.04)[36] suite using the exchange-correlation functional BP86[37] and LanL2DZ[38] (Fe and the C and H atoms of the bridge) and LanL2DZdp[39] (remaining atoms) basis sets obtained from Extensible Computational Chemistry Environment Basis Set Database, Version 02/25/04 (Molecular Science Computing Facility, Pacific Northwest Laboratory, Richland, WA). All geometries are fully optimized and confirmed as minima by an analytical frequency calculation at the same level of theory. DFT-optimized structures are indicated when parentheses enclose the formula used to designate the different species. The validity of the calculated gas-phase geometry may be established by comparison of the calculated and observed IR spectra in the ν(CO) region. Geometry optimization of **4Fe6S** using B3LYP and basis sets described above give structural parameters and ν(CO) band profiles in similarly good agreement with those observed; however the wavenumber offsets for these compounds were found to be smaller when using the BP86 functional. The inclusion of solvation effects provides more accurate estimates of the relative energies of the calculated structures, although a far smaller effect is evident for the calculated geometries and IR spectra. In view of the computational overhead for a problem as complex as that posed by the tetrairon compounds, all calculations reported are for gas-phase species. The crystal structure of **4Fe6S** was used as input for the DFT-based geometry optimization, where the suitability of the approach is demonstrated by the close agreement obtained between the observed and calculated geometry and ν(CO) bands. Geometry optimization of **4Fe6S**$^-$ proceeded from {**4Fe6S**} with the addition of a single electron. The procedure was repeated to give the calculated structure of **4Fe6S**$^{2-}$. In the crystalline form, **4Fe6S** has C_i symmetry[30] and geometry optimization of **4Fe6S**$^{0/-/2-}$ will also give structures with C_i symmetry. Calculations based on a starting geometry with C_1 symmetry refined to give structures indistinguishable from those calculated as described above. Starting geometries for H:**4Fe6S**$^-$ proceeded from {**4Fe6S**$^{2-}$} with placement of the hydrogen atom either at the open coordination site of one of the outer Fe atoms or between an outer and inner pair of Fe atoms. In the latter case, the bridging CO group was placed in the open coordination site of the outer Fe atom.

(30) Tard, C.; Liu, X.; Hughes, D. L.; Pickett, C. J. *Chem. Commun.* **2005**, 133−5.
(31) Armarego, W. L. F.; Perrin, D. D. *Purification of Laboratory Chemicals*, 4th ed.; Butterworth-Heinemann: Oxford, 1996.
(32) Sawyer, D. T.; Sobkowiak, A.; Roberts, J. J. L. *Electrochemistry for Chemists*, 2nd ed.; Wiley-Interscience: New York, 1995.
(33) Nehring, J. L.; Heinekey, D. M. *Inorg. Chem.* **2003**, *42*, 4288−92.
(34) Borg, S. J.; Best, S. P. *J. Electroanal. Chem.* **2002**, *535*, 57−64.
(35) Connelly, N. G.; Geiger, W. E. *Chem. Rev.* **1996**, *96*, 877−910.
(36) Frisch, M. J.; et al. *Gaussian 03*, revision B.04; Gaussian, Inc.: Wallingford, CT, 2004.
(37) Becke, A. D. *Phys. Rev. A* **1988**, *38*, 3098−100. Perdew, J. P. *Phys. Rev. B* **1986**, *33*, 8822−4.
(38) Dunning, T. H., Jr.; Hay, P. J. *Modern Theor. Chem.* **1977**, *3*, 1−27. Hay, P. J.; Wadt, W. R. *J. Chem. Phys.* **1985**, *82*, 270−83. Hay, P. J.; Wadt, W. R. *J. Chem. Phys.* **1985**, *82*, 299−310. Wadt, W. R.; Hay, P. J. *J. Chem. Phys.* **1985**, *82*, 284−98.
(39) Check, C. E.; Faust, T. O.; Bailey, J. M.; Wright, B. J.; Gilbert, T. M.; Sunderlin, L. S. *J. Phys. Chem. A* **2001**, *105*, 8111−6.

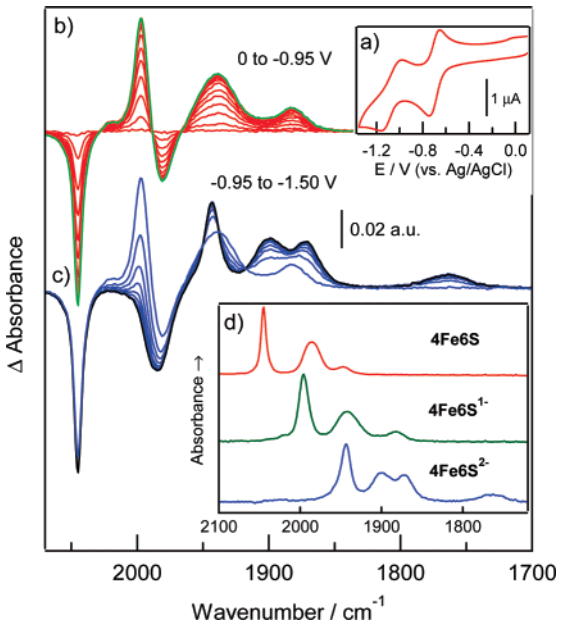

Figure 1. (a) Electrochemistry of **4Fe6S** (1 mM CH_2Cl_2/0.2 M TBA[PF_6]) and IR−SEC spectra after application of a potential of (b) −0.95 V and (c) −1.50 V. The time between spectra is ca. 2 s. (d) The absorbance spectra of the parent compound and the one- and two-electron reduction products, in the latter two cases by spectral subtraction using the SEC spectra.

Results and Discussion

Spectroelectrochemistry. The cyclic voltammetry of **4Fe6S** in CH_2Cl_2 reveals successive reversible and quasi-reversible single-electron reduction steps (Figure 1a).[30] Reversible interconversion between the neutral and anionic forms of **4Fe6S** is well-demonstrated in IR−SEC experiments, where the extent of recovery of the neutral species is near quantitative and not dependent on the reduction time (Figures 1b and S1 of the Supporting Information). Experiments conducted using more reducing potentials show that the dianion of **4Fe6S** is moderately stable at room temperature (Figure 1c), where ca. 95% of the anion can be recovered provided the duration of the reduction step is less than 10 s (Figure S2, Supporting Information). Reduction at longer times results in a more complex band profile consistent with the formation of several as yet undefined decomposition products. The IR spectra of **4Fe6S**$^-$ and **4Fe6S**$^{2-}$ have been extracted from the SEC results by spectral subtraction and these together with the spectrum of the parent compound are shown Figure 1d. Analogous experiments carried out under elevated pressures of CO (0.4 MPa) show that while **4Fe6S**$^-$ is unaffected by additional CO, **4Fe6S**$^{2-}$ undergoes further reaction, leading to a mixture of products (Figure S3, Supporting Information).

The general shift of the ν(CO) band profile lower by ca. 50 cm^{-1} with the addition of each electron is approximately half of that obtained for one-electron reduction of the related diiron compound, **3S**.[16] Further, since there is not a marked increase in the difference between the lowest and highest energy ν(CO) bands for either the anion or dianion, the additional charge is distributed over the four Fe atoms. This conclusion is supported by the magnitude of the shift of the highest energy ν(CO) bands. Furthermore, experiments carried out in the presence of elevated pressures of ^{13}CO show that reduction to the anion results in CO/^{13}CO exchange that continues over a period of ca. 30 s, presumably until the isotopic composition of CO bound to the complex matches that in the thin film of solution (Figure S4, Supporting Information). The lability of the complex to ligand exchange is consistent with its formulation as an odd-electron metal carbonyl species.[40] In addition to supporting the odd-electron assignment of **4Fe6S**$^-$ the isotopic substitution experiments also confirm assignment of the bands in this spectral region to metal carbonyl vibrations.

Table 1. Experimental (**4Fe6S**) and Predicted Bond Lengths for the Redox Series **4Fe6S**$^{0/-/2-}$ and the Terminal Hydride Form of **4Fe6S**$^{2-}$

					{H$_t$:**4Fe6S**$^{2-}$}^{b}	
	4Fe6S^a	{**4Fe6S**}^{b}	{**4Fe6S**$^-$}^{b}	{**4Fe6S**$^{2-}$}^{b}	H:2Fe^c	2Fe^d
$Fe_{outer}-Fe_{inner}$/Å	2.543	2.544	2.582	2.538	2.534	2.535
$Fe_{outer}-S_{outer}$/Å	2.264	2.297	2.305	2.351	2.318	2.350
$Fe_{inner}-Fe_{inner}$/Å	2.651	2.628	2.900	3.467	3.451	
$Fe_{inner}-S_{inner}$/Å	2.236	2.240	2.278	2.333	2.357	2.302
Fe−CO^e/Å	1.791	1.764	1.754	1.728	1.747	1.733
C−O^e/Å		1.173	1.180	1.189	1.176	1.184
$Fe_{inner}-CO_{bridge}$/Å				2.028	1.868	2.078
$Fe_{outer}-CO_{bridge}$/Å				1.855	2.132	1.825
$C-O_{bridge}$/Å				1.203	1.188	1.202

^{a} X-ray distances from ref 30. ^{b} DFT calculated distances. ^{c} Protonated diiron subunit of {H$_t$:**4Fe6S**$^{2-}$}, Fe−H = 1.490 Å. ^{d} Nonprotonated diiron subunit of {H$_t$:**4Fe6S**$^{2-}$}. ^{e} Averaged value.

Similar ν(CO) band profiles are obtained for **4Fe6S** and **4Fe6S**$^-$; however, these differ markedly from that of the dianion (Figure 1d). The appearance of a ν(CO) band at 1780 cm^{-1} for **4Fe6S**$^{2-}$ suggests a rearrangement of the CO groups about the iron−sulfur core with the formation of a product having at least one bridging CO group. The substantial structural change indicated by the IR spectra is fully consistent with the slow heterogeneous electron-transfer kinetics suggested by the quasi-reversible nature of the second reduction wave (Figure 1a).[30]

DFT Studies of the 4Fe6S Redox Series. DFT calculations of the neutral compound yield structural parameters (Table 1) and IR spectrum (Figure 2a) in excellent agreement with that observed. The LUMO is calculated to be Fe−Fe antibonding with respect to the central Fe atoms, and on this basis, reduction would be expected to result in an increase in electron density distributed over both diiron fragments of the molecule. The shift of the entire band profile is consistent with such an analysis. The structure of {**4Fe6S**$^-$} has an elongated central Fe−Fe bond, and the calculated IR spectrum of the anion has a band profile and wavenumber in remarkably good agreement with those observed (Figure 2b). Whereas a further lengthening of the central Fe−Fe contact is expected following formation of {**4Fe6S**$^{2-}$}, it is surprising that this is also accompanied by a rearrangement of the CO groups. One of the terminal CO groups on both outer-Fe atoms is calculated to adopt a position bridging the outer and inner Fe atoms and this leaves an open coordination site on the outer-Fe atoms (Figure 3b). To ascertain the possibility for formation of the all-terminal CO isomer of **4Fe6S**$^{2-}$, geometry optimization was conducted starting from a model with a Fe/S core based on {**4Fe6S**$^{2-}$} and an arrangement of CO groups analogous to that of {**4Fe6S**$^-$}. While no local minimum with an all-terminal CO geometry is obtained, a second-order saddle point, 11.53 kcal mol^{-1} higher in energy than the CO-bridged form, is identified. In this case,

(40) Cotton, F. A.; Wilkinson, G. *Advanced Inorganic Chemistry*, 5th ed.; Wiley-Interscience: New York, 1988.

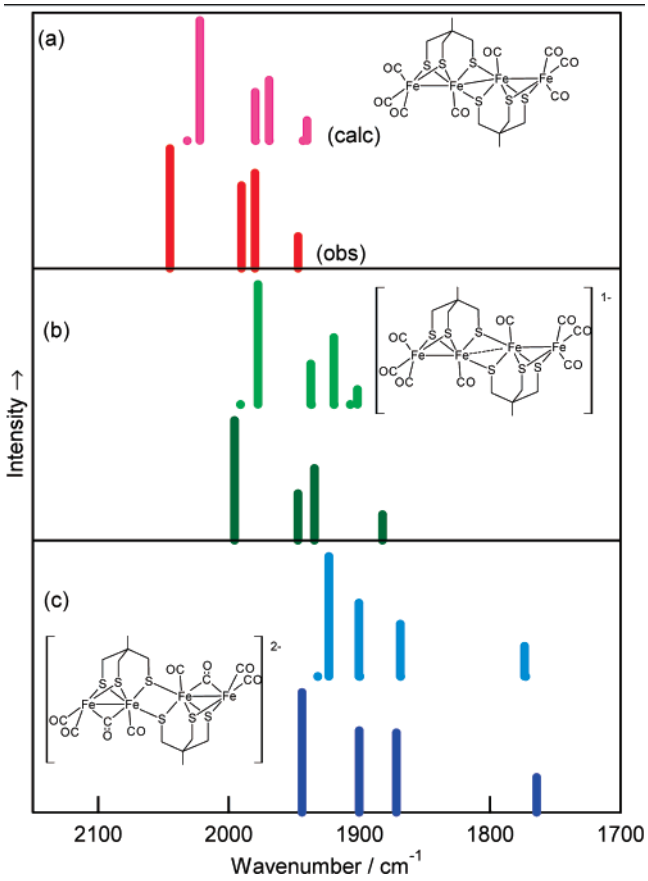

Figure 2. Comparison between the calculated (top) and observed (bottom) ν(CO) bands of (a) **4Fe6S**, (b) **4Fe6S**$^{-}$, and (c) **4Fe6S**$^{2-}$. The experimental intensities were obtained by curve fitting the ν(CO) band profile. The structures of **4Fe6S**$^{-}$ and **Fe6S**$^{2-}$ are based on those obtained by DFT calculation.

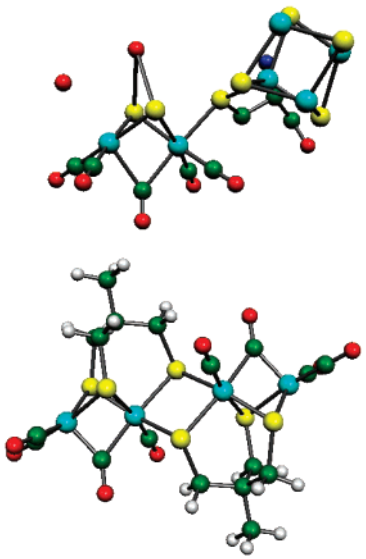

Figure 3. (top) Structure of $\mathbf{H_{ox}}$ as determined by X-ray crystallography of the oxidized form of the [Fe−Fe] hydrogenase from *C. pasteurianum* (PDB ID 1C4A).[2] Note in this published structure the atoms forming the dithiolate bridge were not refined nor assignment of the diatomic ligands as either CO or cyanide made (see Scheme 1). (bottom) DFT-calculated structure of **Fe4S6**$^{2-}$.

the two imaginary frequencies correspond to displacement coordinates that involve a rotation of the $Fe(CO)_3$ fragments and lead, ultimately, to the CO-bridged structure. These calculations suggest that the energy difference between the isomeric forms of {**4Fe6S**$^{2-}$} is significantly larger than the uncertainty in the relative energies introduced by the use of gas-phase calculations (up to 3 kcal mol^{-1}), this being estimated from studies of related diiron compounds.[9] The conclusion that the CO-bridged structure of {**4Fe6S**$^{2-}$} is significantly more stable than the all-terminal CO form is supported by the excellent agreement between the calculated and observed IR spectra (Figure 2c).

The high reactivity of **4Fe6S**$^{2-}$ is readily understood in terms of a CO-bridged structure with open coordination site on the outer Fe atoms, since a similar rearrangement of the all-terminal CO form has previously been invoked to explain the associative character of the substitution reactions. Pickett and co-workers have shown that cyanation of $Fe_2(\mu,\mu\text{-}(SCH_2)_2C(CH_3)(CH_2SR))(CN)(CO)_4$ proceeds through a long-lived CO-bridged intermediate, where transfer of the bridging CO group is coupled to dissociation of the pendant thioether to give the final product.[23]

The striking resemblance between the geometry of the diiron units of {**4Fe6S**$^{2-}$} and the X-ray structure of $\mathbf{H_{ox}}$ from *Clostridium pasteurianum*, CpI,[2] is shown in Figure 3. Both $[2Fe]_{\mathbf{H}_{red}}$ and the inner and outer pair of Fe atoms of {**4Fe6S**$^{2-}$} may have formal oxidation states of either $Fe^{I}Fe^{I}$ or $Fe^{II}Fe^{0}$. In both cases, a change in the mode of coordination of one of the CO groups between terminal and bridging will switch the oxidation state assignment from one alternative to the other. For **4Fe6S**$^{2-}$, the presence of two additional bridging thiolates bound to Fe_{inner} appears to push the equilibrium in favor of the $Fe^{II}Fe^{0}$ form. IR spectroscopy indicates that for $[2Fe]_{\mathbf{H}_{red}}$ all the CO groups adopt a terminal mode of coordination,[5] although the crystallographic structure indicates a hemibridging interaction between CO and Fe_p. DFT calculations indicate that this interaction mixes a significant $Fe^{II}Fe^{0}$ contribution into the ground state.[7] Thus, **4Fe6S**$^{2-}$ presents a close structural and electronic analogue of $\mathbf{H_{red}}$.

Spectroelectrochemistry in the Presence of 2,6-Dimethylpyridinium, LutH^{+}. IR−SEC spectra recorded during the reduction of **4Fe6S** at mild potentials in the presence of 20 equiv of LutH^{+} are shown in Figure 4. The spectral changes closely mirror those obtained for reduction of **4Fe6S** in the absence of acid (Figure 1b), although the rate of depletion of the starting material is lower and weak features due to the conversion of LutH^{+} to Lut become apparent in the spectrum between 1550 and 1700 cm^{-1}. The possibility that proton reduction involves either direct reduction at the electrode surface or is the result of the formation of low concentrations of the dianion was examined in experiments where the potentiostat was switched to open circuit at a time when both LutH^{+} and **4Fe6S**$^{-}$ are present in the thin layer (Figure 4b). Over a period of ca. 50 s there is conversion of all the **4Fe6S**$^{-}$ to **4Fe6S**. The interpretation that the spectral changes observed during this period are due to chemical reaction, as opposed to mixing between the bulk solution and that of the thin layer, is based on the comparatively rapid time scale over which the spectral changes develop. Further, immediately after switching the cell to open circuit, the differential absorption features associated with the conversion of LutH^{+} into its conjugate base, Lut, continue to develop while there is a significant concentration of **4Fe6S**$^{-}$ in the thin layer (Figure 4c). Analogous experiments conducted

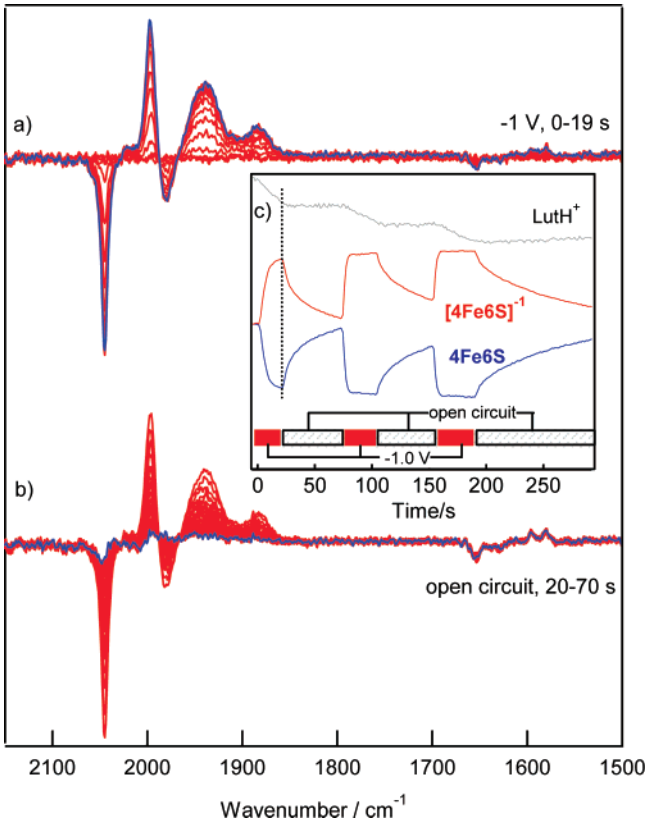

Figure 4. IR−SEC recorded of **4Fe6S** (1.7 mM, CH_2Cl_2/0.2 M TBA[PF_6]) in the presence of $LutH^+$ (34 mM) (a) during the reduction at potentials sufficient to generate the monoanion, (b) the spectral changes obtained after switching the potentiostat to open circuit, and (c) the time dependence of the relative concentrations of $LutH^+$, **4Fe6S**, and **4Fe6S**$^-$ obtained by multicomponent fitting of the individual spectra. The last spectrum of each set shown in a and b is highlighted.

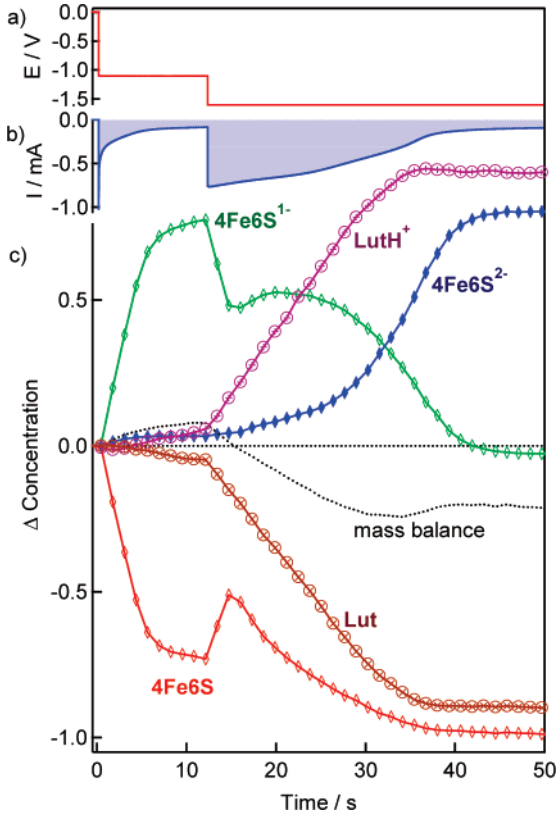

Figure 5. The time dependence of (a) the applied potential, (b) current response, and (c) the time dependence of the concentration changes of **4Fe6S**, **4Fe6S**$^-$, **4Fe6S**$^{2-}$, Lut, and $LutH^+$ during thin-layer SEC of **4Fe6S** (1.1 mM) and $LutH^+$ (38 mM) in CH_2Cl_2 (0.2 M TBA[PF_6]). The concentration changes of Lut and $LutH^+$ have been divided by a factor of 40. The mass balance of **4Fe6S**$^{n-}$ species corresponds to the sum of the concentration changes for **4Fe6S**, **4Fe6S**$^-$, and **4Fe6S**$^{2-}$.

in the absence of acid show that **4Fe6S**$^-$ is stable over the time scale of several minutes and there is no significant spectral change following the switching of the potentiostat to open circuit. The changes in concentration of **4Fe6S**, **4Fe6S**$^-$, and $LutH^+$ during an experiment including three successive reduction/open circuit cycles is shown in **Figure 4c**. With each reduction cycle there is a faster rate of depletion of the starting material and slower rate of its recovery. Both observations may be explained in terms of a lowering of the concentration of $LutH^+$ due to proton reduction in the thin layer of solution. It is important to note that the loss of **4Fe6S**$^-$ through formation of the dianion by disproportionation followed by reaction with acid may be ruled out by the small value of K_{disp} (ca. 10^{-6}). Since in this case formation of the dianion would be rate-limiting, the rate of reaction would be expected to be independent of acid concentration. This analysis is supported by electrochemical simulation of the voltammetry of **4Fe6S** in the presence of acid.[30]

These results show unequivocally that the reduction of protons by **4Fe6S**$^-$ is a kinetically significant process. The absence of additional spectral features during the reaction indicates that there is no buildup of significant concentrations of additional products; consequently, dihydrogen elimination by a bimolecular reaction involving two equivalents of H:**4Fe6S** can be ruled out. A reaction path involving rate-limiting formation of H:**4Fe6S**, reduction by **4Fe6S**$^-$, and rapid reaction of H:**4Fe6S**$^-$ with protons would account for the overall reaction and apparent absence of additional products. On the basis of the equilibrium constants and reduction potentials deduced from modeling the electrochemistry,[30] the equilibrium constant for the protonation of **4Fe6S**$^-$ is estimated to have a value of ca. 10. Complete removal of **4Fe6S**$^-$, as is evident in the SEC experiments, results from removal of the reaction product by irreversible protonation and dihydrogen elimination.

Since dihydrogen evolution following one-electron reduction is limited by the rate of protonation of **4Fe6S**$^-$, the time dependence of the spectral changes obtained after switching the potentiostat to open circuit provides a means of estimating the rate constant for the protonation reaction. For the first cycle an observed rate constant (k_{obs}) of 0.25 ± 0.01 s^{-1} is obtained from fitting the spectral changes for depletion of **4Fe6S**$^-$ and recovery of **4Fe6S** over the first half-life after switching the potentiostat to open circuit. For rate-limited protonation, k_{obs} will equal the product of the second-order rate constant for the protonation of **4Fe6S**$^-$ (k_1) and the concentration of $LutH^+$. The estimated value of k_1 of 9 ± 2 M^{-1} s^{-1} is in satisfactory agreement with that previously deduced from digital simulation of the electrochemistry (25 M^{-1} s^{-1}).[30]

The relative rates of electrocatalysis for the two reduction processes is apparent from the time and potential dependence of the spectral changes during thin layer SEC experiments of **4Fe6S** with 35 equiv of $LutH^+$. Reduction at mild potentials leads to a modest current response, and this is associated with conversion of a significant fraction of the neutral compound

Scheme 2. Possible Structures of H:**4Fe6S**$^{-}$

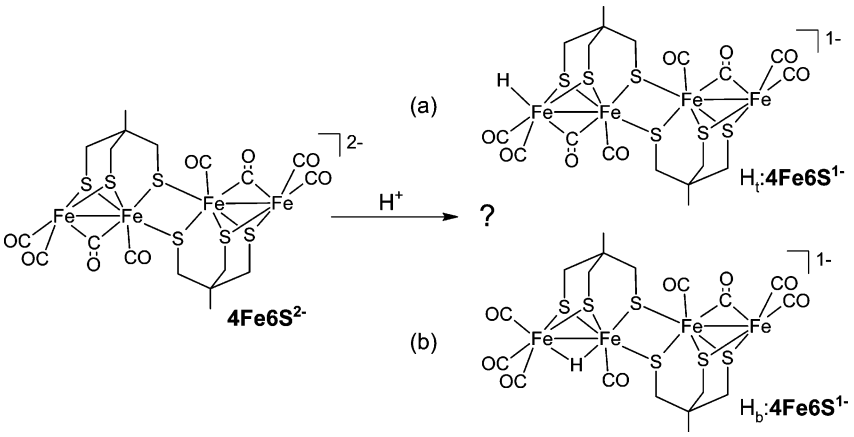

into the one-electron reduced form (Figure 5). Since the turnover on protons is slow, the predominant species in solution is **4Fe6S**$^{-}$. In the second stage of the reaction the potential is stepped to a value sufficiently reducing to access the dianion, and this is associated with a marked increase in the rate of depletion of $LutH^+$ together with an *increase* in the concentration of the neutral compound and concomitant decrease in concentration of **4Fe6S**$^{-}$ (Figure 5). This surprising situation may be explained in terms of the relative rates of recovery of **4Fe6S** by reaction of **4Fe6S**$^{2-}$ and **4Fe6S**$^{-}$ with $LutH^+$. Analogous experiments conducted with differing acid concentrations and for different periods of reduction at -1.1 V suggest that the extent of transient recovery of **4Fe6S** after switching the potential to -1.6 V depends on the residual acid concentration. Despite the rapid turnover on protons following two-electron reduction, comproportionation of **4Fe6S**$^{2-}$ and **4Fe6S** in the thin layer provides a means of generating significant concentrations of **4Fe6S**$^{-}$. Only when the concentration of **4Fe6S** is small does **4Fe6S**$^{2-}$ become the predominant product (Figure 5). Following the application of more strongly reducing potentials, the mass balance of **4Fe6S**$^{n-}$ species (Figure 5) indicates the formation of low concentrations of other metal-based species. It is clear that these species do not play a significant role in the catalytic reaction, since there is no delay in the onset of the full catalytic current following the step in potential. Rearrangement of protonated reduced compounds has previously been found to accompany the electrocatalytic reaction, and this is responsible for the loss of catalyst from the system.[16] It has not proved possible to obtain well-defined spectra of these products.

Digital simulation of the respective electrocatalytic proton reduction reactions suggests that the rate of dihydrogen elimination following two-electron, two-proton addition is substantially higher for **4Fe6S** (2000 s^{-1})[41] than either **3P** (2.4 s^{-1})[28] or **3S** (5 s^{-1}).[16] This order of reactivity is surprising, since the hydridic character of the species may be expected to be enhanced as the complex is reduced and the formal oxidation states of the iron atoms is higher for **4Fe6S** than for **3S** or **3P**. This suggests a different reaction path for electrocatalytic proton reduction by **4Fe6S**. Since the reaction path for rapid proton reduction by **4Fe6S** involves net two-electron reduction prior to protonation, it is likely that the structural rearrangement accompanying formation of **4Fe6S**$^{2-}$ is central to the increased reactivity. Both the opening of a coordination site on the outer iron atom and the development of Fe^0Fe^{II} centers would promote the proton basicity and hydridic character needed to facilitate such a reaction.

A possible reaction path available to **4Fe6S**$^{2-}$ and not the diiron compounds is for protonation to occur on the inner iron atoms and for both diiron fragments of H_2:**4Fe6S** to be directly involved in dihydrogen elimination. However, this reaction path may be excluded on the basis of the calculated Fe−Fe distance (Table 1). Recent theoretical[29] and experimental[28] studies of **3S** and **3P** suggest that electrocatalytic proton reduction proceeds via dihydrogen elimination from a Fe_A:Fe_B dihydride, where the rate of dihydrogen elimination is related to the H−H distance, this being related to the Fe_A−Fe_B separation.[28] The calculated structure of the H_2:**4Fe6S** isomer having the inner Fe atoms protonated has a Fe_{inner}−Fe_{inner} distance (3.447 Å) little changed from that of {**4Fe6S**$^{2-}$} (Table 1) and an H−H distance of 4.273 Å. A similar Fe−Fe distance is obtained for **DP**$^{2-}$, and in that case, the dihydride does not eliminate dihydrogen at a significant rate.[26]

Therefore, dihydrogen elimination from H_2:**4Fe6S** is centered on one of the Fe_{outer}−Fe_{inner} fragments with the remaining diiron fragment available to provide an additional reducing equivalent. Protonation of **4Fe6S**$^{2-}$ may occur at the open coordination site of one of the outer iron atoms or, alternatively, at the inner iron atom, where this is coupled with a rearrangement of the bridging CO group (Scheme 2). These alternatives mirror the latter stages of the paths of dihydrogen oxidation proposed for the H-cluster (Scheme 1).

Dihydrogen elimination from a dihydride obtained by protonation of a species such as H_b:**4Fe6S**$^{-}$ may, in view of the shorter Fe_{outer}−Fe_{inner} separation, be expected to support a faster rate of dihydrogen elimination than the corresponding species of **3S** and **3P**; however, the oxidation states of the iron atoms is higher and this may be expected to lower the basicity of the H-bridged species. Crystallographically characterized hydride-bridged $Fe^{II}Fe^{II}$ species have been obtained by protonation of the disubstituted Fe^IFe^I phosphines[25] to give $[Fe_2(\mu\text{-pdt})(\mu\text{-H})(PR_3)_2(CO)_4]^+$ and by hydride addition to the $Fe^{II}Fe^{II}$ precursor of **2SH$_b$**$^+$.[42] In neither case is there any indication of significant

(41) The value of the rate constant for dihydrogen elimination was not given explicitly in ref 30. The value reported is obtained by fitting the voltammetry to a model consistent with those used in refs 28 and 16.

(42) Zhao, X.; Georgakaki, I. P.; Miller, M. L.; Mejia-Rodriguez, R.; Chiang, C.-Y.; Darensbourg, M. Y. *Inorg. Chem.* **2002**, *41*, 3917−28.

proton basicity, even in the presence of acids significantly stronger than $LutH^+$.

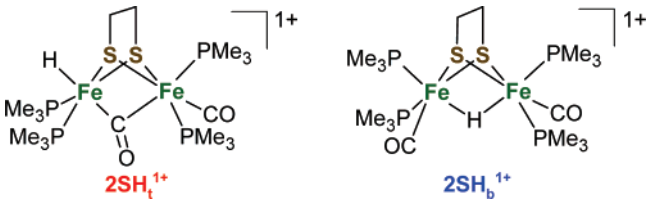

Terminally bound hydrides are known for thiolate- and phosphido-bridged diiron compounds, although the hydridic character of these diiron species is markedly different. Whereas $\mathbf{2SH_t}^+$ reacts with acid to eliminate dihydrogen, $[Fe_2(\mu\text{-}PPh_2)_2H(CO)_6]^-$ is unreactive. In the latter case, the IR spectra indicate that the two iron centers are weakly interacting and the hydride formulation would imply binding to an Fe^{II} center.[26] The difference in ligand set and stronger electronic interaction between the Fe^{II} centers of $\mathbf{2SH_t}^+$ would appear to promote the hydridic character of the terminally bound hydride. Similar considerations apply for H_t:**4Fe6S**$^-$, where the outer and inner iron atoms are bridged both by a dithiolate and a CO group as for $\mathbf{2SH_t}^+$ and, notably, $\mathbf{H_{ox}}$. The hydridic character of the tetrairon complex may be further enhanced by redistribution of charge from the remote pair of iron centers. Geometry optimization of H:**4Fe6S**$^-$ starting from the protonated form of **4Fe6S**$^{2-}$ corresponding to H_t:**4Fe6S**$^-$ (Scheme 2a) proceeds to a well-defined energy minimum, as judged by the calculated vibrational frequencies. The structure retains a terminal hydride and bridging CO group. These calculations suggest that the bridging CO group moves from a position closer to Fe_{outer} for the dianion to one closer to Fe_{inner} for {H_t:**4Fe6S**$^-$}, while there is a smaller shift of the bridging CO toward Fe_{outer} for the nonprotonated subunit (Table 1).

DFT-based geometry optimization of H_b:**4Fe6S**$^-$ (Scheme 2b) gives a similarly well-behaved minimum with a calculated gas-phase free energy 0.75 kcal mol^{-1} lower than that of {H_t:**4Fe6S**$^-$}, well within the uncertainty of the calculation. Further work is needed to establish whether there is a sufficiently large difference in the calculated activation energies to provide an unequivocal basis for distinguishing between the two reaction paths. These calculations would have clear parallels with those conducted on the enzyme.[14]

Conclusion

The application of SEC approaches has allowed identification of the IR spectra of the **4Fe6S**, **4Fe6S**$^-$, and **4Fe6S**$^{2-}$ redox series. Whereas the ν(CO) band pattern is largely retained following one-electron reduction, there are significant changes associated with formation of **4Fe6S**$^{2-}$, most notably the appearance of a ν(CO) band at 1764 cm^{-1} indicative of the presence of at least one CO group adopting a bridging mode of coordination.

DFT-based geometry optimization of **4Fe6S** gives structural parameters and IR spectra in excellent agreement with those observed. The LUMO is calculated to be antibonding with respect to the inner Fe atoms, and one-electron reduction is manifested by a lengthening of this bond. Addition of a second electron is calculated to give a further lengthening of the Fe_{inner}−Fe_{inner} distance and, unexpectantly, a rearrangement of the CO groups about the **4Fe6S** core. The calculated geometry consists of two identical diiron units with an open coordination site on Fe_{outer} and a bridging CO group on Fe_{outer} and Fe_{inner}. These features of the structure are unprecedented in dithiolate-bridged diiron chemistry outside the [Fe−Fe] hydrogenase enzyme.

Electrocatalytic proton reduction proceeds slowly at mild potentials by one-electron reduction of **4Fe6S**, rate-limiting protonation, further one-electron reduction, and dihydrogen elimination. A dramatic increase in the rate of electrocatalysis occurs if two-electron reduction precedes protonation. The structural rearrangement associated with formation of **4Fe6S**$^{2-}$ provides a diiron unit, which is closely related to $\mathbf{H_{red}}$ sharing (i) an accessible Fe^0Fe^{II} redox level with an open coordination site on the Fe^0 center and (ii) a thiolate bridge to a second redox center able to provide a second electron during proton reduction to give a final oxidized Fe^IFe^{II} form. These features of the chemistry clearly require differentiation of the coordination environments of the Fe centers of the diiron unit.

While further calculations are needed to establish unequivocally that an alternate reaction path of **4Fe6S** can be dismissed, consideration of the structures of the compounds, their relation to electrocatalytic proton reduction by **3S** and **3P**, and the difference in rate of dihydrogen elimination following protonation of $\mathbf{2SH_t}^+$ and $\mathbf{2SH_b}^+$ suggest formation of a terminal hydride (H_t:**4Fe6S**, Scheme 2a) and a reaction path analogous to the reverse of Scheme 1a. While lacking the CO/CN$^-$ substitution pattern and including two, instead of one, bridging thiolate sulfur atoms to a second redox center, **4Fe6S** nevertheless provides important insights into the reaction path of the H cluster and for the design of new electrocatalysts.

Note Added in Proof. A paper published after submission of the manuscript (Ezzaher, S.; Capon, J.-F.; Gloaguen, F.; Pétillon, F. Y.; Schollhammer, P.; Talarmin, J.; Pichon, R.; Kervarec, N. *Inorg. Chem.* **2007**, *46*, 3426−8) shows that protonation of the asymmetrically substituted diiron(I) compound $Fe(\mu\text{-}S(CH_2)_3S)CO_4(dppe)$, dppe = $Ph_2PP(CH_2)_2PPh_2$, proceeds through a terminally bound hydride en route to the more stable hydride-bridged form. This observation provides further support for a reaction path for **4Fe6S** that involves a terminally bound hydride (Scheme 2a).

Acknowledgment. The work was supported by grants from the Australian Research Council (S.P.B. and C.J.P.), BBSRC (C.J.P.), the John Innes Centre (where the earlier work was initiated), and the EPSRC (Supergen 5, C.J.P.). M.H.C. and C.T. acknowledge the University of Melbourne and the John Innes Foundation, respectively, for the award of scholarships. Support of the Victorian Institute for Chemical Sciences High Performance Computing Facility is gratefully acknowledged.

Supporting Information Available: Full ref 36, IR−SEC showing recovery of **4Fe6S** from **4Fe6S**$^-$ and **4Fe6S**$^{2-}$, IR−SEC of **4Fe6S**$^{2-}$ under 0.4 MPa CO and **4Fe6S**$^-$ under 0.4 MPa ^{13}CO, Cartesian coordinates from DFT calculations, and frequencies and intensities of DFT-calculated species. This material is available free of charge via the Internet at http://pubs.acs.org.

JA071331F